J Syst Sci Complex (2021) 34: 520–536

A Second-Order Sliding Mode Controller of Quad-Rotor UAV Based on PID Sliding Mode Surface with Unbalanced Load*

KANG Bing · MIAO Yan · LIU Fu · DUAN Jilu · WANG Ke · JIANG Shoukun

DOI: 10.1007/s11424-020-9306-6
Received: 5 November 2019 / Revised: 22 December 2019

Abstract Quad-rotor unmanned aerial vehicle (UAV) is a typical multiple-input-multiple-output underactuated system with couplings and nonlinearity. Usually, the flying environment is very complex, so that it is impossible for the UAV to avoid effects derived from disturbances and uncertainties. In order to improve the reliability of flight control, we established the dynamic model of quad-rotor UAV by Newton-Euler equation in unbalanced load conditions. Considering external disturbances in the attitude, a second-order sliding mode controller was designed with PID sliding mode surface and Extended State Observer (ESO). The simulation experiments have got good control performance, illustrating the effectiveness of our controller. Meanwhile, the controller was implemented in a quad-rotor UAV, which carried a pan-tilt camera for aerial photography. The actual flight experiments proved that this paper dealt with the high stabilization flight control problem for the quad-rotor UAV, which laid a good foundation for autonomous flight of the UAV.

Keywords Quad-rotor UAV, sliding mode controller, unbalanced load.

1 Introduction

With the rapid development of MEMS (micro-electro-mechanical system), micro sensors, micro-processors, new materials, flight control, machine vision and other technologies, the rapid rise of quad-rotor unmanned aerial vehicle (UAV) is promoted. Quad-rotor UAV is playing a more and more powerful role in anti-terrorism, traffic monitoring[1], disaster relief[2], express transportation, environmental monitoring[3] and auxiliary scientific research[4], etc. These application scenarios all put forward strong requirements for UAVs load capacity, and these loads are often unbalanced loads. In addition, external interference, air resistance, model uncertainty, gyroscopic moment and other factors also seriously affect the performance of UAV. Therefore, it

KANG Bing · MIAO Yan · LIU Fu (Corresponding author) · DUAN Jilu · WANG Ke · JIANG Shoukun
College of Communication Engineering, Jilin University, Changchun 130022*, China.*
Email: liufu@jlu.edu.cn.
*This research was supported by the National Natural Science Foundation of China under Grant No. 61503151.
◇ *This paper was recommended for publication by Editor SUN Jian.*

becomes a key issue in control field about how to make the UAV fly steadily under unbalanced load.

There have been numerous methods to control the flying stability of quad-rotor UAV, including both linear and nonlinear control. Conventional PID (proportion integration differentiation) control[5] and LQ control[6], two naive linear control techniques, are simple and flexible in structure and convenient in the real-time application, both of which, however, rely heavily on the accuracy of their physical models and have defects in the robustness of the system. Nonlinear control techniques such as backstepping control[7] and feedback linearization[8] have the ability to solve the nonlinearity and coupling of the quad-rotor UAV model, but are lack of the ability of disturbance rejection. To deal with these defects, some nonlinear control methods have been developed such as adaptive control[9, 10], neural network control[11], robust control[12], sliding mode control[13, 14], and so on. They not only improved the nonlinear problem of UAV system, but also considered the uncertainty of the system, which could enhance the control accuracy of the actual system.

Different from the general quad-rotor UAV, the flight of loaded UAV may be greatly affected by the back and forth swing of the load, which may even cause the UAV to be out of control with too intense swing. Researches on the loaded quad-rotor UAV cover a relatively wide range, from 2D plane modeling[15–17] to 3D all-round modeling[18, 19], from single quad-rotor UAV transportation to multi quad-rotor UAVs cooperative transportation[20–23], from solid load with a constant center of mass to liquid load with changing center of mass[24], all of which, however, lack the consideration of the load with seriously unbalance.

In this paper, the control strategy of quad-rotor UAV with unbalanced load was studied. A modified dynamic model of quad-rotor UAV was presented based on the Newton-Euler equation in the condition of unbalanced load. The disturbance of unbalance load was regarded as translational system. According to the dynamic equation, we designed a second-order sliding mode controller with PID sliding mode surface based on extended state observer (ESO). For the attitude control of UAV, the ESO-based second-order sliding mode controller was combined with the robust control and adaptive control to reduce the jitter caused by unbalanced load. The simulation experiments and actual flight experiments all got good control performance under unbalanced load, which illustrated the effectiveness of our controller.

2 Mechanical Model and Kinematic Equations of Quad-Rotor UAV

2.1 Mechanical Model

In the progress of flight, a quad-rotor UAV is under the action of several forces including the gravity $m_1 g$ of the UAV itself, the lift forces F_i generated by propellers, the air resistance force and the air friction force, and three moments including aerodynamic moment M_i caused by propellers' lift, counter moment caused by rotation and gravity moment caused by barycenter offset. Simply, the air resistance and air friction force are omitted here in the process of flight. The force diagram is plotted in Figure 1.

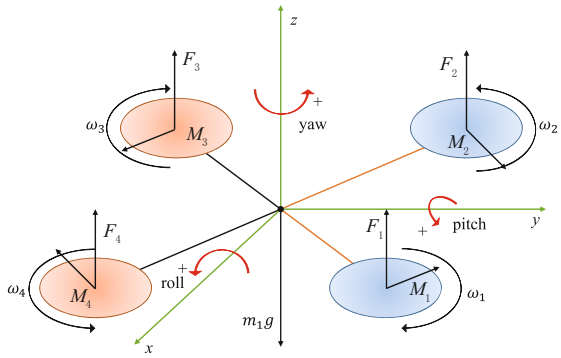

Figure 1 The force diagram of a quad-rotor UAV

The lift force generated by a propeller is defined as:

$$F = \frac{1}{2}CS\rho\omega^2, \tag{1}$$

where C describes the coefficient of the lift force which is related to geometric parameters of the propeller; S represents the projection area on the ground of a propeller; ρ is the air density; ω represents the velocity of a propeller. When hovering, the forces acting on a quad-rotor UAV have a balanced relationship as shown in Equation (2):

$$F_1 + F_2 + F_3 + F_4 = m_1 g, \tag{2}$$

where F_1, F_2, F_3 and F_4 represent the lift forces generated by four propellers; m_1 is the mass of the UAV. To make the balance of moments between X-axis and Y-axis, Equation (3) ought to be satisfied as well:

$$\begin{cases} (F_1 + F_4)\dfrac{l}{\sqrt{2}} = (F_2 + F_3)\dfrac{l}{\sqrt{2}}, \\ (F_1 + F_2)\dfrac{l}{\sqrt{2}} = (F_3 + F_4)\dfrac{l}{\sqrt{2}}, \end{cases} \tag{3}$$

where l is the distance between the center of a propeller and the origin of the axis. The antitorque is calculated as Equation (4):

$$M_i = J_i \mathrm{d}\omega_i/\mathrm{d}t, \quad 1 \le i \le 4, \tag{4}$$

where J_i and ω_i are moment of inertia and angular velocity of the ith propeller respectively. Hence Equation (5) should be satisfied to keep hovering:

$$M_1 - M_2 + M_3 - M_4 = 0. \tag{5}$$

Above all, a hovering quad-rotor UAV needs to meet the requirement of Equation (6):

$$\begin{cases} F_1 + F_2 + F_3 + F_4 = m_1 g, \\ M_1 + M_3 = M_2 + M_4, \\ F_1 = F_3, \\ F_2 = F_4. \end{cases} \tag{6}$$

2.2 Kinematic Equations

In the condition of ignoring the influence of the air resistance and air friction, the lift forces $F_{x'}$, $F_{y'}$, and $F_{z'}$ in body axis system are:

$$\begin{bmatrix} F_{x'} \\ F_{y'} \\ F_{z'} \end{bmatrix} = \begin{bmatrix} 0 \\ 0 \\ F_1 + F_2 + F_3 + F_4 \end{bmatrix}. \tag{7}$$

The matrix $R(\varphi, \theta, \psi)$ representing the orientation of the body-fixed frame relative to the earth-fixed inertial frame are expressed as:

$$R(\varphi, \theta, \psi) = \begin{bmatrix} \cos\psi cos\varphi & \cos\psi\sin\theta\sin\varphi - \sin\psi\sin\varphi & \cos\psi\sin\theta\cos\varphi + \sin\psi\sin\varphi \\ \sin\psi\cos\theta & \sin\psi\sin\theta\sin\varphi - \cos\psi\cos\varphi & \sin\psi\sin\theta\cos\varphi - \sin\psi\sin\varphi \\ -\sin\theta & \cos\theta\sin\varphi & \cos\theta\cos\varphi \end{bmatrix}. \tag{8}$$

The lift forces in earthfixed inertial frame can be calculated by the transition matrix $R(\varphi, \theta, \psi)$ as:

$$\begin{bmatrix} F_x \\ F_y \\ F_z \end{bmatrix} = R(\varphi, \theta, \psi) \begin{bmatrix} F_{x'} \\ F_{y'} \\ F_{z'} \end{bmatrix} = \sum_{i=1}^{4} F_i \begin{bmatrix} \cos\psi\sin\theta\cos\varphi + \sin\psi\sin\varphi \\ \sin\psi\sin\theta\cos\varphi - \sin\psi\sin\varphi \\ \cos\theta\cos\varphi \end{bmatrix} = m_1 \begin{bmatrix} \ddot{S}_x \\ \ddot{S}_y \\ \ddot{S}_z + g \end{bmatrix}, \tag{9}$$

where F_x, F_y and F_z are components of the lift force along X-axis, Y-axis and Z-axis; S_x, S_y and S_z are the displacements along X-axis, Y-axis and Z-axis, respectively; φ, θ and ψ are the rotation angles of UAV around the X-axis, Y-axis and Z-axis respectively. The rotation equation in the progress of flight is calculated as Equation (10):

$$\begin{bmatrix} J_x\ddot{\varphi} \\ J_y\ddot{\theta} \\ J_z\ddot{\psi} \end{bmatrix} = \begin{bmatrix} (F_1 + F_2 - F_3 - F_4)\frac{l}{\sqrt{2}} \\ (F_2 + F_3 - F_1 - F_4)\frac{l}{\sqrt{2}} \\ M_1 - M_2 + M_3 - M_4 \end{bmatrix}, \tag{10}$$

where, J_x, J_y and J_z are moments of three axes. Therefore, the kinematic equation of the quad-rotor UAV is shown as Equation (11):

$$\begin{cases} \ddot{S}_x = \dfrac{1}{m}(\cos\psi\sin\theta\cos\varphi + \sin\psi\sin\varphi)(F_1 + F_2 + F_3 + F_4), \\ \ddot{S}_y = \dfrac{1}{m}(\sin\psi\sin\theta\cos\varphi - \sin\psi\sin\varphi)(F_1 + F_2 + F_3 + F_4), \\ \ddot{S}_z = \dfrac{1}{m}(\cos\theta\cos\varphi)(F_1 + F_2 + F_3 + F_4) - g, \\ \ddot{\varphi} = \dfrac{1}{\sqrt{2}J_x}(F_1 + F_2 - F_3 - F_4), \\ \ddot{\theta} = \dfrac{1}{\sqrt{2}J_y}(-F_1 + F_2 + F_3 - F_4), \\ \ddot{\psi} = \dfrac{1}{J_z}(M_1 - M_2 + M_3 - M_4). \end{cases} \tag{11}$$

3 Mechanical Analysis of Quad-Rotor UAV with Unbalanced Load

3.1 Estimation of UAV's Center of Gravity Position with Unbalanced Load

Under unbalanced load, the modification of UAV dynamic model is determined by the coordinate of center of gravity $G(x_d, y_d, 0)$, which is estimated by the attitude parameters of UAV as following during takeoff:

$$\begin{cases} x_d = \dfrac{\ddot{\varphi}_d}{m_0 g \cos \varphi_d}, \\ y_d = \dfrac{\ddot{\theta}_d}{m_0 g \cos \theta_d}, \end{cases} \tag{12}$$

where m_0 is the quality of load; g is the acceleration of gravity; φ_d and θ_d describe the rotation angles of UAV around the X-axis and Y-axis respectively.

3.2 Mechanical Model

For the sake of simplicity, the air resistance and air friction force in the process of flight are omitted in this paper. The center of gravity lies in the geometric center of the UAV without load. A gravity added to an axis leads to the effect of unbalanced load, as shown in Figure 2.

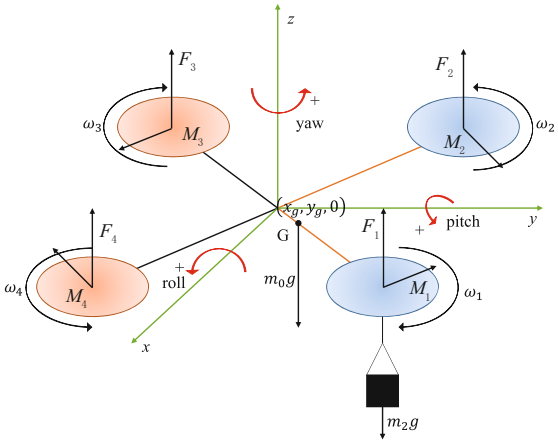

Figure 2 The force diagram of a UAV with unbalanced load

$G(x_d, y_d, 0)$ instead of $O(0, 0, 0)$ in a conventional situation represents the current position of the center of gravity. In hover, the moment balance equations around X-axis and Y-axis are:

$$\begin{cases} (F_1 + F_4)\dfrac{l}{\sqrt{2}} = (F_2 + F_3)\dfrac{l}{\sqrt{2}} + m_0 g * x_d, \\ (F_1 + F_2)\dfrac{l}{\sqrt{2}} = (F_3 + F_4)\dfrac{l}{\sqrt{2}} + m_0 g * y_d, \end{cases} \tag{13}$$

where F_1, F_2, F_3 and F_4 are lift forces generated by four propellers; l is the distance between the center of a propeller and $O(0, 0, 0)$. Therefore, the unbalancedly loaded UAV needs to meet

the requirement of Equation (14):

$$\begin{cases} F_1 + F_2 + F_3 + F_4 = m_0 g = (m_1 + m_2)g, \\ F_1 = F_3 + m_0 g * (x_d + y_d)\dfrac{1}{\sqrt{2}l}, \\ F_4 = F_2 + m_0 g * (x_d - y_d)\dfrac{1}{\sqrt{2}l}, \\ M_1 + M_3 = M_2 + M_4, \end{cases} \tag{14}$$

where m_2 is the mass of the load; m_1 is the mass of the UAV; m_0 is the mass of the whole system including load; M_i is the reaction torque generated during rotation that is equal in amount and opposite in direction to the relative torque generated by motors.

The angular velocities of the four propellers are calculated as Equation (15):

$$\begin{cases} \omega_1 = \omega_0 + \dfrac{m_0 g(x_d + y_d)}{4\sqrt{2}\omega_0 H l}, \\ \omega_2 = \omega_0 - \dfrac{m_0 g(x_d - y_d)}{4\sqrt{2}\omega_0 H l}, \\ \omega_3 = \omega_0 - \dfrac{m_0 g(x_d + y_d)}{4\sqrt{2}\omega_0 H l}, \\ \omega_4 = \omega_0 + \dfrac{m_0 g(x_d - y_d)}{4\sqrt{2}\omega_0 H l}, \end{cases} \tag{15}$$

where ω_0 is the average of the angular velocity; H, an intrinsic parameter of the propeller, is the distance that the UAV has traveled in a circle of rotor rotation.

3.3 Attitude Estimation

For a convenient attitude settlement, the attitude of the quad-rotor UAV is jointly settled by quaternion and Euler angle. The attitude change of UAV can be expressed by the angle of the fuselage rotating around the axis of rotation. The quaternion $q = (w, i, j, k)^{\mathrm{T}}$ is satisfied as:

$$q^2 = w^2 + i^2 + j^2 + k^2 = 1, \tag{16}$$

where the vector $(i, j, k)^{\mathrm{T}}$ represents the rotation axis; w describes the angle of rotation around the rotation axis. According to the mathematical relationship between Euler angle and quaternion, the formula for converting quaternions to Euler angles is as follows:

$$\begin{bmatrix} \varphi \\ \theta \\ \psi \end{bmatrix} = \begin{bmatrix} \arctan\left(\frac{2(wi+jk)}{1-2(i^2+j^2)}\right) \\ \arcsin\left(2\left(wj - ik\right)\right) \\ \arctan\left(\frac{2(wk+ij)}{1-2(j^2+k^2)}\right) \end{bmatrix}, \tag{17}$$

where φ, θ and ψ are the rotation angles of UAV around the X-axis, Y-axis and Z-axis respectively.

3.4 Kinematic Analysis of UAV with Unbalanced Load

In a relatively ideal condition, the rotation equation in the progress of flight is calculated as Equation (18):

$$\begin{bmatrix} J_x\ddot{\varphi} \\ J_y\ddot{\theta} \\ J_z\ddot{\psi} \end{bmatrix} = \begin{bmatrix} (F_1+F_2-F_3-F_4)\frac{l}{\sqrt{2}} - m_0 g \cdot y_d \\ (F_2+F_3-F_1-F_4)\frac{l}{\sqrt{2}} + m_0 g \cdot x_d \\ M_1 - M_2 + M_3 - M_4 \end{bmatrix}. \tag{18}$$

According to the analysis above, the kinematic equations of the quad-rotor UAV with unbalanced load is shown as Equation (19):

$$\begin{cases} \ddot{S}_x = \dfrac{1}{m_1}(\cos\psi\sin\theta\cos\varphi + \sin\psi\sin\varphi)(F_1+F_2+F_3+F_4), \\ \ddot{S}_y = \dfrac{1}{m_1}(\sin\psi\sin\theta\cos\varphi - \sin\psi\sin\varphi)(F_1+F_2+F_3+F_4), \\ \ddot{S}_z = \dfrac{1}{m_1}(\cos\theta\cos\varphi)(F_1+F_2+F_3+F_4) - g, \\ \ddot{\varphi} = \dfrac{1}{\sqrt{2}J_x}(F_1+F_2-F_3-F_4) - m_0 g \cdot y_d/J_x, \\ \ddot{\theta} = \dfrac{1}{\sqrt{2}J_y}(-F_1+F_2+F_3-F_4) + m_0 g \cdot x_d/J_y, \\ \ddot{\psi} = \dfrac{1}{J_z}(M_1 - M_2 + M_3 - M_4). \end{cases} \tag{19}$$

4 Design of the Controller

To solve that the conventional second-order sliding mode controller meets a problem of fluctuation leading to poor stability in flight, an ESO-based second-order sliding mode controller with PID sliding mode surface is proposed. As a part of active disturbance rejection controller (ADRC), the ESO[25] is extensively used to estimate the expanded state of the system dynamically by the original input-output information. The observed real-time actions are equivalent to the sum of all kinds of disturbances (from modelling, unmodeled dynamics and external disturbances) acting on the integrator series system. With this estimation, a real-time dynamic compensation is carried out to realize the system linearization. The progress of control is plotted in Figure 3.

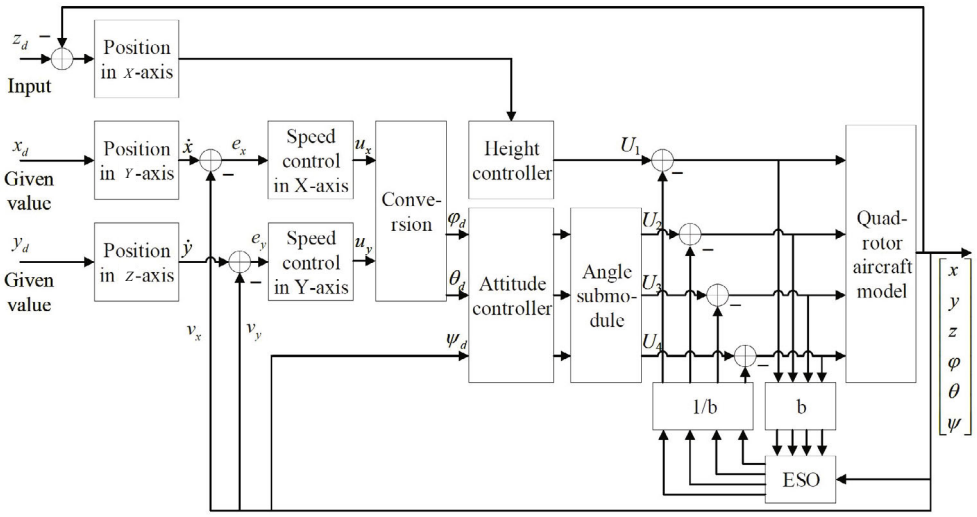

Figure 3 The diagram of the control system block

4.1 Construction of the Extended State Observer for Quad-Rotor UAV with Unbalanced Load

The errors e_x and e_y of the velocities were calculated as Equation (20). They were the differences between the velocities $\dot{x}$ and $\dot{y}$ calculated from relative position to the target and the current velocities v_x and v_y respectively, which were the inputs to the PID controller. The expected velocities u_x and u_y from the output of PID controller were inputted to the conversion module, from which the expected roll angle φ_d and pitch angle θ_d (as Equation (22)) were outputted to the attitude controller.

$$\begin{cases} e_x = \dot{x} - v_x, \\ e_y = \dot{y} - v_y, \end{cases} \tag{20}$$

$$\begin{cases} u_x = k_P e_x + k_I \int e_x + k_D \dot{e}_x, \\ u_y = k_P e_y + k_I \int e_y + k_D \dot{e}_y, \end{cases} \tag{21}$$

where, $k_{Pi}, k_{Ii}, k_{Di} \in R^+$ are the coefficients of proportionality, integration and differential, respectively, all of which are integral constants.

$$\begin{cases} \varphi_d = \arcsin\left(u_x \sin\psi - u_y \cos\psi\right), \\ \theta_d = \arcsin\left(\dfrac{u_x}{\cos\varphi\cos\psi} - \dfrac{\sin\varphi\sin\psi}{\cos\varphi\cos\psi}\right). \end{cases} \tag{22}$$

The output of the height controller U_1 is used to control the height of the quad-rotor UAV, and the outputs of the angle submodule after attitude controller U_2, U_3, U_4 are used to control the attitude stability of the UAV. For the sake of simplicity, the height channel is used to explain the specific mathematical realization of the structure.

Combined with the equation in state space, the height z is rewrited as:

$$\begin{cases} \dot{\varsigma}_1 = \varsigma_2, \\ \dot{\varsigma}_2 = f_1(\varphi, \dot{\varphi}, \theta, \dot{\theta}, \psi, \dot{\psi}) + d_1 + b_1 U_1, \\ z = \varsigma_1, \end{cases} \tag{23}$$

where, b_1 is the coefficient of control quantity; d_1 is the disturbance of unbalanced load. $a = f_1(\varphi, \dot{\varphi}, \theta, \dot{\theta}, \psi, \dot{\psi}) + d_1$ is defined as the sum of all kinds of disturbances (from modeling, unmodeled dynamics and external disturbances), and the total disturbance is regarded as an unknown expanded state variable, that is $\varsigma_3 = a$. Hence, Equation (23) becomes:

$$\begin{cases} \dot{\varsigma}_1 = \varsigma_2, \\ \dot{\varsigma}_2 = \varsigma_3 + b_1 U_1, \\ \dot{\varsigma}_3 = \omega_1. \\ z = \varsigma_1 \end{cases} \tag{24}$$

A nonlinear ESO is then established for the above system:

$$\begin{cases} e = \widehat{\varsigma}_1 - z, \\ \dot{\widehat{\varsigma}}_1 = \widehat{\varsigma}_2 - \beta_1 e, \\ \dot{\widehat{\varsigma}}_2 = \widehat{\varsigma}_3 - \beta_2 fal(e, a_1, \delta) + b_1 U_1, \\ \dot{\widehat{\varsigma}}_3 = -\beta_3 fal(e, a_2, \delta), \end{cases} \tag{25}$$

where,

$$fal(e, a_i, \delta) = \begin{cases} |e|^{a_i} \text{sign}(e), & |e| > \delta, \\ e/\delta^{-a_i}, & |e| \le \delta, \end{cases} \qquad i = 1, 2;$$

$a_1 = 0.5$, $a_2 = 0.25$[26], and appropriate hyperparameters β_1, β_2, β_3 ($\beta_1 = \beta_2 = \beta_3 = 80$ in this paper) are commonly chosen here. Then the output $\widehat{\varsigma}_3$ of the ESO is infinitely close to $\varsigma_3 = f_1(\varphi, \dot{\varphi}, \theta, \dot{\theta}, \psi, \dot{\psi}) + d_1$. Although the specific expressions of $f_1(\varphi, \dot{\varphi}, \theta, \dot{\theta}, \psi, \dot{\psi})$ and d_1 are unknown, the total disturbance of the system can be well estimated by the extended state $\widehat{\varsigma}_3$. Similarly, the dynamic compensation linearization of the other three channels (the channel of yaw angle, pitch angle, and roll angle specifically) can be realized by the same treatment, which can greatly improve the system's resistance to unbalanced load.

4.2 Design of the ESO-Based Second-Order Sliding Mode Controller with PID Sliding Mode Surface

The second-order PID sliding mode surface is chosen as:

$$\dot{s}_i + \beta s_i = k_{Pi} e_i + k_{Ii} \int_0^t e_i dt + k_{Di} \dot{e}_i, \quad i = 1, 2, 3, 4, \tag{26}$$

where, sliding mode variables $s_i = \varepsilon_{ci} e_i + \dot{e}_i$; $\beta \in R^+$ is a hyperparameter; e_1, e_2, e_3 and e_4 are the errors between real height, yaw angle, pitch angle, roll angle and their expectations;

ε_{ci} needs to meet the Hurwitz criterion that $\varepsilon_{ci} > 0$. To overcome the chattering of signal function that affects the performance of the whole system, the saturation function[27] is utilized as following:

$$sat\,(s_i) = \begin{cases} s_i, & \text{if } |s_i| \le 1, \\ \text{sign}\,(s_i), & \text{if } |s_i| > 1, \end{cases} \quad i = 1, 2, 3, 4, \tag{27}$$

where the index approach rates $\dot{s}_i = -k_{ci} sat\,(s_i)$ $(k_{ci} > 0)$.

The Lyapunov function $V_{(i)}$[28] is chosen as:

$$V_{(i)} = \frac{1}{2} s_i^2 + \frac{1}{2} \dot{s}_i^2. \tag{28}$$

It is clear that $V_{(i)}(0) = 0$; when $s_i \neq 0$ and $\dot{s}_i \neq 0$, $V_{(i)} > 0$. Then the derivation of Equation (28) is:

$$\dot{V}_{(i)} = s_i \dot{s}_i + \ddot{s}_i \dot{s}_i. \tag{29}$$

Combined with Equation (26), Equation (29) becomes:

$$\begin{aligned} \dot{V}_{(i)} &= s_i \dot{s}_i + \dot{s}_i \left[-k_{Di} d_i - k_{Di} b_i \varepsilon_i s_i - k_{Di} b_i k_{si} sign\,(\dot{s}_i) \right] \\ &= s_i \dot{s}_i - k_{Di} b_i \varepsilon_i s_i \dot{s}_i - \dot{s}_i k_{Di} d_i - k_{Di} b_i k_{si} \left| \dot{s}_i \right| \\ &= - \left| s_i \dot{s}_i \right| \left[-1 + k_{Di} b_i \varepsilon_i \right] - \left| \dot{s}_i \right| \left[k_{Di} d_i + k_{Di} b_i k_{si} \right], \end{aligned} \tag{30}$$

when the unsettling limit of the equation is written as:

$$d_i^+ = - \left| s_i \dot{s}_i \right| \left[-1 + k_{Di} b_i \varepsilon_i \right] - \left| \dot{s}_i \right| \left[k_{Di} d_i + k_{Di} b_i k_{si} \right] \tag{31}$$

with the limitation of $k_{si} > -\frac{d_i}{b_i}$, $s_i \neq 0$, $\dot{s}_i \neq 0$, $|s_i| > 0$, $|\dot{s}_i| > 0$.

It can be seen that in the condition of the limitation above, $d_i^+ < 0$, which means the lyapunov function is negative definite. Therefore, the closed-loop system is globally asymptotically stable, so all the trajectories of the system can reach and eventually stay on the sliding mode surface.

When it comes to the control of height,

$$e_1 = z_d - z, \tag{32}$$

$$\ddot{s}_1 + \beta \dot{s}_1 = k_{P1} \dot{e}_1 + k_{P1} e_1 + k_{D1} \ddot{e}_1, \tag{33}$$

$$\ddot{z} = -g + (\cos\varphi \cos\theta) \frac{1}{m} U_1. \tag{34}$$

Combined with Equation (25), the control strategy is:

$$U_1 = \frac{m}{\cos\varphi \cos\theta k_{D1}} \left\{ k_{P1} \left(\dot{z}_d - z \right) + k_{I1} \left(z_d - z \right) + k_{D1} \left(\ddot{z}_d + g \right) - \beta \dot{s}_1 \right\} - \frac{\widehat{\varsigma}_{3z}}{b_1}. \tag{35}$$

Similarly, the complete control strategies are:

$$\begin{cases} U_1 = \dfrac{m}{\cos\varphi\cos\theta k_{D1}}\left\{k_{P1}\left(\dot{z}_d - z\right) + k_{I1}\left(z_d - z\right) + k_{D1}\left(\ddot{z}_d + g\right) - \beta\dot{s}_1\right\} - \dfrac{\widehat{\varsigma}_{3z}}{b_1}, \\ U_2 = \dfrac{1}{b_2 k_{D2}}\left\{k_{D2}\left(\dot{\varphi}_d - \dot{\varphi}\right) + k_{I2}\left(\varphi_d - \varphi\right) + k_{D2}\left(\ddot{\varphi}_d - \dot{\theta}\dot{\psi}a_1 - \dot{\theta}a_2\Omega\right) - \beta\dot{s}_2\right\} - \dfrac{\widehat{\varsigma}_{3\varphi}}{b_2}, \\ U_3 = \dfrac{1}{b_3 k_{D3}}\left\{k_{P3}\left(\dot{\theta}_d - \dot{\theta}\right) + k_{I3}\left(\theta_d - \theta\right) + k_{D3}\left(\ddot{\theta}_d - \dot{\varphi}\dot{\psi}a_3 - \dot{\varphi}a_4\Omega\right) - \beta\dot{s}_3\right\} - \dfrac{\widehat{\varsigma}_{3\theta}}{b_3}, \\ U_4 = \dfrac{1}{b_4 k_{D4}}\left\{k_{P4}\left(\dot{\psi}_d - \dot{\psi}\right) + k_{I4}\left(\psi_d - \psi\right) + k_{D3}\left(\ddot{\psi}_d - \dot{\theta}\dot{\varphi}a_5\right) - \beta\dot{s}_4\right\} - \dfrac{\widehat{\varsigma}_{3\psi}}{b_4}, \end{cases} \tag{36}$$

where $\widehat{\varsigma}_{3z}$, $\widehat{\varsigma}_{3\varphi}$, $\widehat{\varsigma}_{3\theta}$, $\widehat{\varsigma}_{3\psi}$ are extended states from ESO of height, roll angle, piych angle, and yaw angle, respectively.

5 Experiments and Results

5.1 Simulations

Before simulating, the parameters of the quad-rotor UAV were measured according to the real hardware (DJI M100) as shown in Table 1, and then used to model a simulated quad-rotor UAV in Simulink.

Table 1 Parameters measured from DJI M100

Symbol	Definition	Value	Unit
m_0, m_1, m_2	Mass	1.5	Kg
I_x	Moment along X-axis	0.41	Kg·m^2
I_y	Moment along Y-axis	0.41	Kg·m^2
I_z	Moment along Z-axis	0.62	Kg·m^2
J	Body moment	0.31	Kg·m^2
l	Distance from center of mass to motor	0.25	m
g	Gravitational acceleration	9.8	N/Kg

5.1.1 Comparison on the Performance of Attitude Controlling Without Any Load

To prove the effectiveness of proposed controller, the conventional PID controller and second order sliding mode controller were used to make a comparison on the performance of attitude controlling. The step response curves of height, yaw angle, pitch angle and roll angle are shown in Figure 4, where the Y-axes represent their corresponding outputs, and the X-axes represent the time. The overshoot of three methods are shown in Table 2.

In terms of height control, our proposed controller almost had none overshoot, much better than the PID controller and conventional second order slide mode controller (SOSC in Figure 4), which were 20% and 10% respectively, meaning a better performance for the step response signal. Also in terms of angles of yaw, pitch and roll, our proposed controller had a similar performance as that of height, being a slight or even none overshoot.

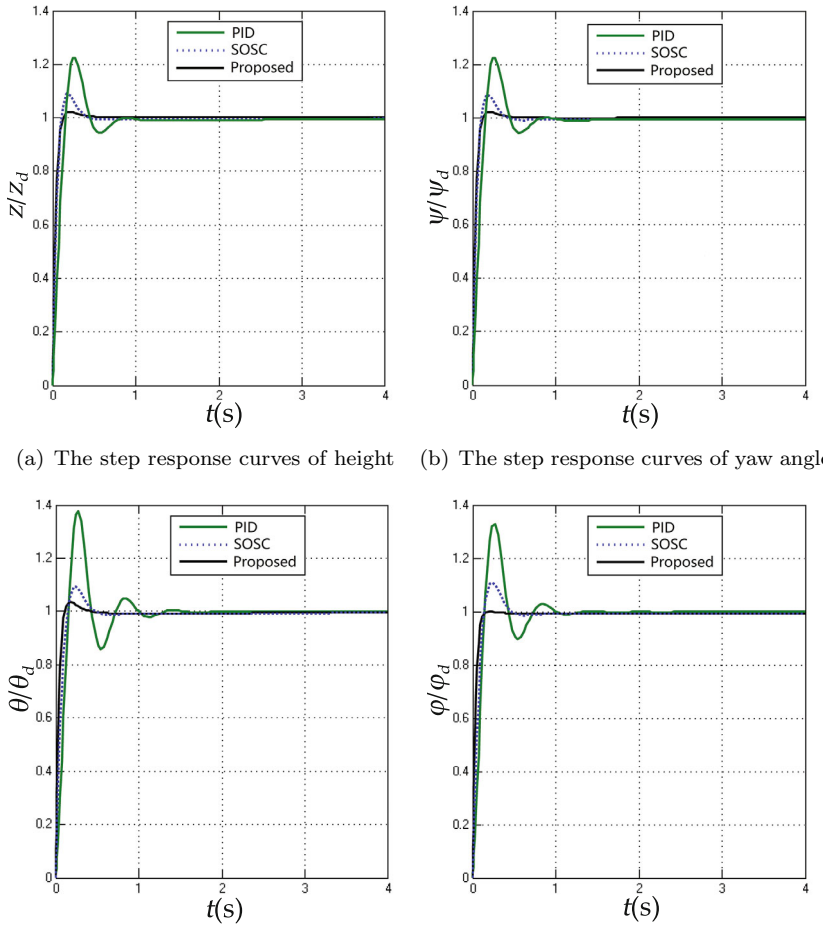

(a) The step response curves of height (b) The step response curves of yaw angle

(c) The step response curves of pitch angle (d) The step response curves of roll angle

Figure 4 The step response curves in the condition without load

Table 2 The overshoot of three methods in the condition of being unloaded

Controller	PID controller	Conventional second order slide mode controller	Proposed controller
Overshoot of height	21.88%	9.93%	1.62%
Overshoot of yaw angle	22.09%	9.41%	1.21%
Overshoot of pitch angle	37.67%	10.43%	3.03%
Overshoot of roll angle	32.12%	13.29%	0.55%

5.1.2 Comparison on the Performance of Attitude Controlling with Unbalanced Load

As what had been done in the situation of non-loaded flight, the conventional PID controller and second order sliding mode controller were used to make a comparison on the performance of unbalanced-loaded UAV's attitude controlling. The step response curves of height, yaw angle,

pitch angle and roll angle are shown in Figure 5, where the Y-axes represent their corresponding outputs, and the X-axes represent the time. The overshoot of three methods are shown in Table 3.

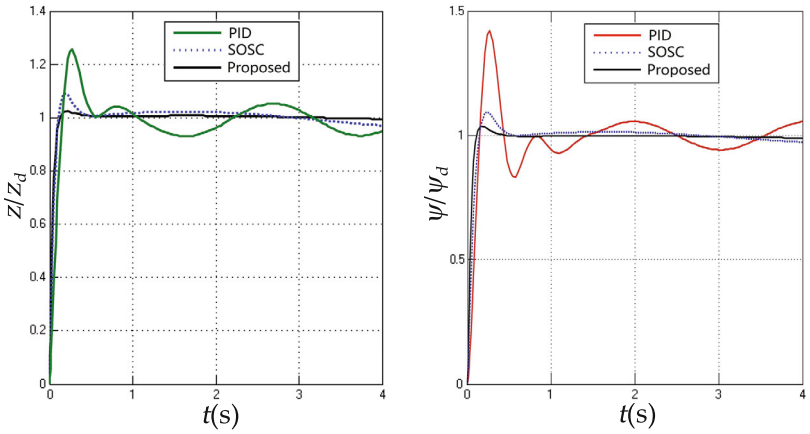

(a) The step response curves of height

(b) The step response curves of yaw angle

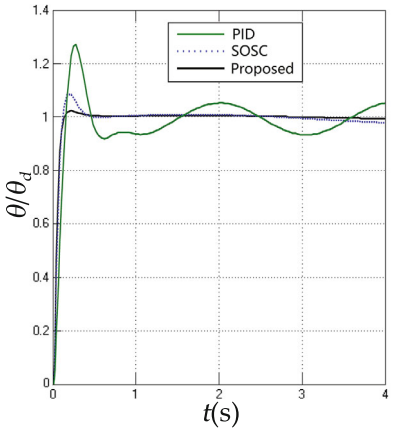

(c) The step response curves of pitch angle

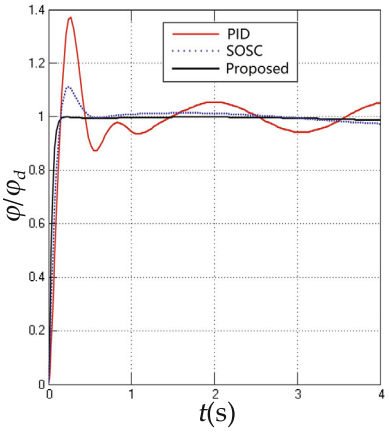

(d) The step response curves of roll angle

Figure 5 The step response curves in the condition with unbalanced load

Table 3 The overshoot of three methods in the condition of unbalanced load

Controller	PID controller	Conventional second order slide mode controller	Proposed controller
Overshoot of height	25.32%	10.68%	1.21%
Overshoot of yaw angle	41.77%	13.54%	3.89%
Overshoot of pitch angle	28.11%	9.67%	1.43%
Overshoot of roll angle	38.55%	12.49%	0.16%

Given a step signal of height to the controller of UAV with unbalanced load, it is clear to be seen that there was about 25% overshoot of PID with a continuous shock. The overshoot of the

second order sliding mode controller (SOSC in Figure 5) was about 10% with a slight shock. However in terms of our proposed controller, the overshoot was reduced to 3% and the stable state was almost not influenced, which was much better than both of the two compared methods above. When it comes to angles of yaw, pitch and roll, our proposed controller outperformed the other two as well.

5.2 Actual Flight Experiments

A 0.185kg-mass counterpoise as a load was tied to one of four rotors of the quad-rotor UAV, DJI M100, by a 15 cm long string before flight. The distance between the load and the center of the UAV was set to be 15 cm. The mass of the UAV itself was 1.5 kg. When the UAV was rising up, the oscillogram was generated as plotted in Figure 6. The blue, black, green and yellow lines represented height, pitch angle, roll angle and displacement along X-axis, respectively. Clearly, there was little overshoot in height response curve with almost no fluctuation. The time used for rising and regulating was at a short level and the errors were within the allowable range. And the result of fixed altitude flight experiment is shown in Figure 7. The change of roll angle and pitch angle during flight is shown in Figure 8.

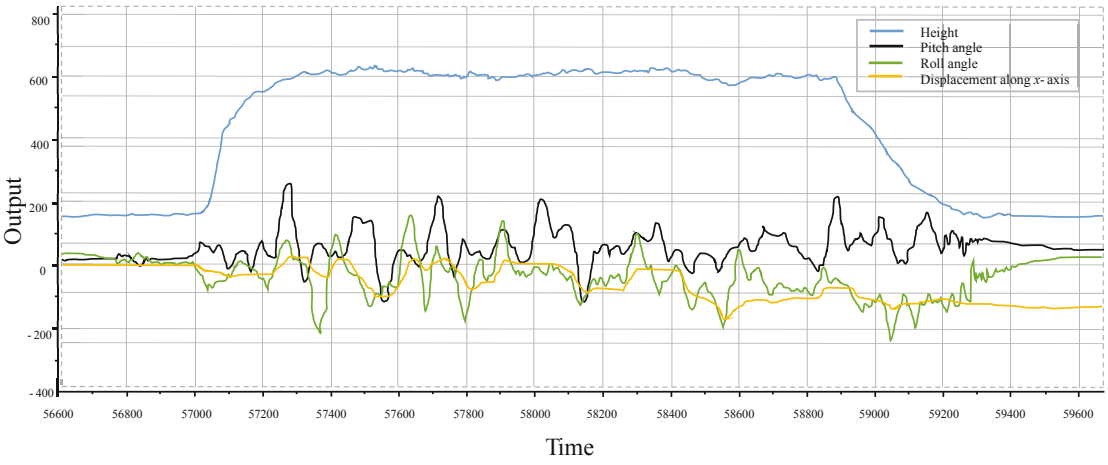

Figure 6 Oscillogram in the progress of flight with unbalanced load

It can be seen from the response curves of pitch angle and roll angle that the attitude data of the UAV fluctuate with unbalanced load. There are two reasons for this kind of fluctuation: on the one hand, the unbalanced load affects the stable flight of the UAV during take-off in a certain continuity; on the other hand, as the unbalanced load is hung on the UAV by the string, the shaking of the weight affects the flight of the UAV, leading to a certain vibration of the flight attitude. However, the experimental results show that this range of oscillation is acceptable, which does not affect the stable flight of the UAV.

Above all, the precision and the speed of the response both reached to a relatively high level, proving the effectiveness and applicability of our proposed controller when the UAV was unbalancedly loaded.

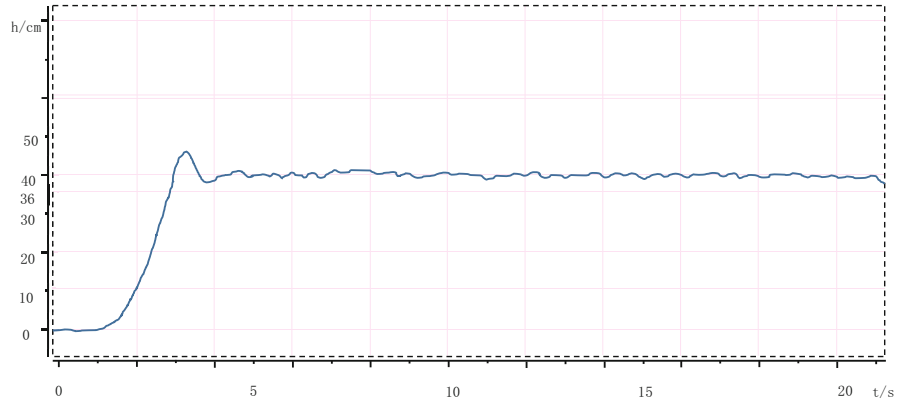

Figure 7 Curve of fixed altitude flight

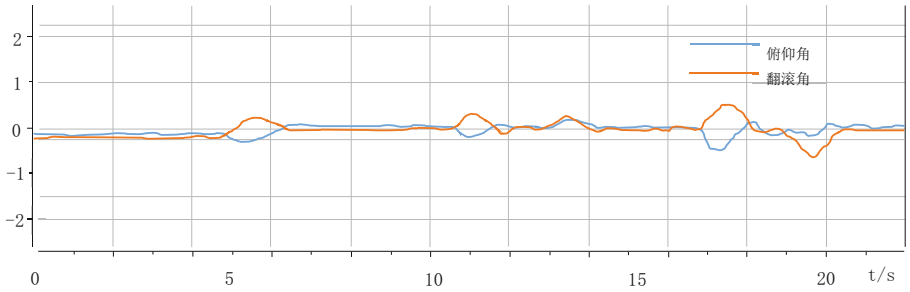

Figure 8 Curves of roll angle and pitch angle during flight

6 Conclusion

In this paper, a modified dynamic model is presented for quad-rotor UAV with unbalanced load. According to conventional PID control and sliding mode control, a PID based second order sliding controller is proposed to weaken the effect of unbalanced load on the system's stability. Additionally, the ESO combined with the robust control and adaptive control is added to the controller so that the jitter caused by unbalanced load can be reduced. Both simulations and practical experiments have shown that our proposed controller has a significant improvement than both conventional PID control and sliding mode control.

References

[1] Zhou HL, Kong H, Wei L, et al., Efficient road detection and tracking for unmanned aerial vehicle, *IEEE Transactions on Intelligent Transportation Systems*, 2015, **16**(1): 297–309.

[2] Nedjati A, Vizvari B, and Izbirak G, Post-earthquake response by small UAV helicopters, *Natural Hazards*, 2016, **80**(3): 1669–1688.

[3] Giannetti F, Chirici G, Gobakken T, et al., A new approach with DTM-independent metrics for forest growing stock prediction using UAV photogrammetric data, *Remote Sensing of Environment*, 2018, 195–205.

[4] Hodgson A, Kelly N, and Peel D, Unmanned aerial vehicles (UAVs) for surveying marine fauna, *A Dugong Case Study, Plos One*, 2013, **8**(11): e79556.

[5] Zhu J C, Liu E D, Guo S, et al., A Gradient Optimization based PID Tuning Approach on Quadrotor, *Proceeding of the* 27*th Chinese Control and Decision Conference* (*CCDC*), Qingdao, China, 2015, 1588–1593.

[6] Bouabdallah S, Noth A, and Siegwart R, PID vs LQ control techniques applied to an indoor micro quadrotor, *Proceedings of IEEE/RSJ International Conference on Intelligent Robots and Systems Sendai, Japan*, 2004, **3**: 2451–2456.

[7] Chen F Y, Lei W, Zhang K K, et al., A novel nonlinear resilient control for a quadrotor UAV via backstepping control and nonlinear disturbance observer, *Nonlinear Dynamics*, 2016, **85**(2): 1281–1295.

[8] Palunko I and Fierro R, Adaptive control of a quadrotor with dynamic changes in the center of gravity, *Proceedings of the* 18*th IFAC World Congress*, Milan, 2011, 2626–2631.

[9] Li S S, Wang Y N, and Tan J H, Adaptive and robust control of quadrotor aircrafts with input saturation, *Nonlinear Dynamics*, 2017, **89**(1): 255–265.

[10] Tian B L, Cui J, Lu H C, et al., Adaptive finite-time attitude tracking of quadrotors with experiments and comparisons, *IEEE Transactions on Industrial Electronics*, 2019, **66**(12): 9428–9438.

[11] Dierks T and Jagannathan S, Output feedback control of a quadrotor UAV using neural networks, *IEEE Transactions on Neural Networks*, 2010, **21**(1): 50–66.

[12] Liu H, Li D J, Zuo Z Y, et al., Robust attitude control for quadrotors with input time delays, *Control Engineering Practice*, 2017, **58**: 142–149.

[13] Zou Y, Nonlinear robust adaptive hierarchical sliding mode control approach for quadrotors, *International Journal of Robust and Nonlinear Control*, 2017, **27**(6): 925–941.

[14] Nafia N, El Kari A, Ayad H, et al., Robust full tracking control design of disturbed quadrotor uavs with unknown dynamics, *Aerospace*, 2018, **5**(4): 115.

[15] Nicotra M M, Garone E, Naldi R, et al., Nested saturation control of a UAV carrying a suspended load, *American Control Conference*, Portland, Oregon, USA, 2014, 3585–3590.

[16] Pizetta I H B, Brandao A S, and Sarcinelli-Filho M, Cooperative quadrotors carrying a suspended load, *International Conference on Unmanned Aircraft Systems*, Arlington, VA, USA, 2016, 1049–1055.

[17] Cruz P J, Oishi M, and Fierro R, Lift of a cable-suspended load by a quadrotor: A hybrid system approach, *American Control Conference*, Chicago, IL, USA, 2015, 1887–1892.

[18] Guerrero M E, Mercado D A, Lozano R, et al., Passivity based control for a quadrotor UAV transporting a cable-suspended payload with minimum swing, *IEEE Conference on Decision and Control*, Osaka, Japan, 2015, 6718–6723.

[19] Alothman Y, Jasim W, and Gu D, Quad-rotor lifting-transporting cable-suspended payloads control, *International Conference on Automation and Computing*, Glasgow, UK, 2015, 1–6.

[20] Lee T, Geometric control of multiple quadrotor UAVs transporting a cable-suspended rigid body, *IEEE Conference on Decision and Control*, Los Angeles, CA, USA, 2014, 6155–6160.

[21] Wu G and Sreenath K, Geometric control of multiple quadrotors transporting a rigid-body load,

IEEE Conference on Decision and Control, Los Angeles, CA, USA, 2014, 6141–6148.

[22] Lee T, Sreenath K, and Kumar V, Geometric control of cooperating multiple quadrotor UAVs with a suspended payload, *IEEE Conference on Decision and Control*, Florence, Italy, 2013, 5510–5515.

[23] Maza I, Ollero A, Casado E, et al., Classification of multi-UAV architectures, *Handbook of Unmanned Aerial Vehicles*, 2014, 953–975.

[24] Sayyaadi H and Soltani A, Modeling and control for cooperative transport of a slung fluid container using quadrotors, *Chinese Journal of Aeronautics*, 2018, **31**(2): 62–72.

[25] Zhang D Y, Wu Q H, and Yao X L, Bandwidth based stability analysis of active disturbance rejection control for nonlinear uncertain systems, *Journal of Systems Science and Complexity*, 2018, **31**(6): 1449–1468.

[26] Guo Y J, Yu L, and Xu J M, Robust finite-time trajectory tracking control of wheeled mobile robots with parametric uncertainties and disturbances, *Journal of Systems Science and Complexity*, 2019, **32**(5): 1358–1374.

[27] Runcharoon K and Srichatrapimuk V, Sliding mode control of quadrotor, *Proc., IEEE Int. Conf. on Technological Advances in Electrical, Electronics and Computer Engineering*, New York, 2013, 552–557.

[28] Chen Q, Tao L, and Nan Y R, Full-order sliding mode control for high-order nonlinear system based on extended state observer, *Journal of Systems Science and Complexity*, 2016, **29**(4): 978–990.